

# AN 84- $\mu$ G MAGNETIC FIELD IN A GALAXY AT $Z=0.692$

ARTHUR M. WOLFE<sup>1</sup> and REGINA A. JORGENSEN,

Department of Physics and Center for Astrophysics and Space Sciences;

University of California, San Diego;

La Jolla, CA; 92093-0424

awolfe@ucsd.edu, regina@physics.ucsd.edu

TIMOTHY ROBISHAW and CARL HEILES

Astronomy Department;

University of California;

Berkeley, CA; 94720-3411

robishaw@astro.berkeley.edu, heiles@astro.berkeley.edu

and

JASON X. PROCHASKA

UCO-Lick Observatory;

University of California, Santa Cruz

Santa Cruz, CA; 95464

xavier@ucolick.org

Received \_\_\_\_\_; accepted \_\_\_\_\_

The magnetic field pervading our Galaxy is a crucial constituent of the interstellar medium: it mediates the dynamics of interstellar clouds, the energy density of cosmic rays, and the formation of stars <sup>1</sup>. The field associated with ionized interstellar gas has been determined through observations of pulsars in our Galaxy. Radio-frequency measurements of pulse dispersion and the rotation of the plane of linear polarization, i.e., Faraday rotation, yield an average value  $B \approx 3 \mu\text{G}$  (ref. 2). The possible detection of Faraday rotation of linearly polarized photons emitted by high-redshift quasars <sup>3</sup> suggests similar magnetic fields are present in foreground galaxies with redshifts  $z > 1$ . As Faraday rotation alone, however, determines neither the magnitude nor the redshift of the magnetic field, the strength of galactic magnetic fields at redshifts  $z > 0$  remains uncertain. Here we report a measurement of a magnetic field of  $B \approx 84 \mu\text{G}$  in a galaxy at  $z = 0.692$ , using the same Zeeman-splitting technique that revealed an average value of  $B = 6 \mu\text{G}$  in the neutral interstellar gas of our Galaxy <sup>4</sup>. This is unexpected, as the leading theory of magnetic field generation, the mean-field dynamo model, predicts large-scale magnetic fields to be weaker in the past rather than stronger. <sup>5</sup>

We detected Zeeman splitting of the  $z=0.692$ , 21 cm absorption line in the direction of the quasar 3C 286 (refs. 6,7) using the 100-m Robert C. Byrd Green Bank Telescope (GBT) of the National Radio Astronomy Observatory. The absorption arises in a damped Ly $\alpha$  system (henceforth denoted DLA-3C286) that is drawn from a population of neutral gas layers widely thought to be the progenitors of modern galaxies <sup>8</sup>. The radio data for DLA-3C286 are summarized in Fig. 1, which shows the line-depth spectra constructed from the measurable quantities used to describe polarized radiation, that is, the Stokes parameters. We show the line-depth spectra constructed from the  $I(\nu)$  and  $V(\nu)$  Stokes parameters (where  $\nu$  denotes frequency) near the 839.4 MHz frequency

centroid of the redshifted 21 cm absorption line. Fig. 1a shows the line-depth spectrum constructed from  $I(\nu)$ . A Gaussian fit to the absorption line in Fig. 1a yields a redshift  $z=0.6921526\pm 0.0000008$ , central optical depth of  $\tau_0=0.095\pm 0.006$ , and a velocity dispersion  $\sigma_v=3.75\pm 0.20 \text{ km s}^{-1}$ , which are in good agreement with previous results <sup>6,7</sup>.

In Fig. 1b we plot the line-depth spectrum constructed from  $V(\nu)$ , which shows the classic ‘S curve’ pattern expected for Zeeman splitting. From our least squares fit to the data, we find  $B_{\text{los}}=83.9\pm 8.8 \mu\text{G}$ , where  $B_{\text{los}}$  is the magnetic field component projected along the line of sight (we note that the direction of  $B_{\text{los}}$  is unknown since the instrumental sense of circular polarization was not calibrated). This magnetic field differs in two respects from the magnetic fields obtained from Zeeman splitting arising in interstellar clouds in the Galaxy. First, the field strength corresponds to the line-of-sight component of the mean field  $\langle B_{\text{los}} \rangle$  averaged over transverse dimensions exceeding 200 pc, as very-long-baseline interferometry observations of the 21-cm absorption line show that the gas layer must extend across more than 0.03 " to explain the difference between the velocity centroids of the fringe amplitude and phase-shift spectra <sup>9</sup> (although the data are consistent with a  $B$ -field coherence length less than 200 pc, the resulting gradient in magnetic pressure would produce velocity differences exceeding the shift of  $\approx 3 \text{ km s}^{-1}$  across 200 pc detected by very-long-baseline interferometry). By contrast, the transverse dimensions of radio beams subtended at neutral interstellar clouds in the Galaxy are typically less than 1 pc. Second, this field is at least an order of magnitude stronger than the 6- $\mu\text{G}$  average of  $B$  fields inferred from Zeeman splitting for such clouds <sup>4</sup>.

We obtained further information about conditions in the absorbing gas in DLA-3C286 from accurate optical spectra acquired with the HIRES Echelle spectrograph on the Keck I 10 m telescope. Fig. 2 shows velocity profiles for several resonance absorption lines arising from dominant low-ionization states of abundant elements. The results of our least squares

fit of Voigt profiles to the data are shown in Table 1, where the optical redshift is displaced  $+3.8 \pm 0.2 \text{ km s}^{-1}$  from the 21 cm redshift. This solution also yields ionic column densities from which we derived the logarithmic metal abundances with respect to solar abundances,  $[M/H]$ , and dust-to-gas ratios with respect to the Galactic interstellar medium,  $[D/G]$ . These are among the lowest values of  $[M/H]$  and  $[D/G]$  deduced for damped  $\text{Ly}\alpha$  systems at  $z=0.7$  (refs. 10, 11). The low metallicity indicates a history of low star formation rates (SFR). Because the intensity of far ultra-violet radiation emitted by young massive stars is proportional to the concurrent SFR per unit area  $\Sigma_{\text{SFR}}$ , low values of  $\Sigma_{\text{SFR}}$  should result in low grain photoelectric heating rates per H atom,  $\Gamma_{\text{pe}}$  (ref. 11). This is consistent with the low upper limit,  $\Gamma_{\text{pe}} < 10^{-27.4} \text{ ergs s}^{-1}$  per hydrogen atom, obtained by combining the assumption of thermal balance with the absence of C II\* absorption (that is, absorption from C II in the excited  $^2P_{3/2}$  fine structure state) at a wavelength of  $1335.7 \text{ \AA}$  in the previous low-resolution Hubble Space Telescope (HST) spectra of 3C 286 (ref. 12), and indicates  $\Sigma_{\text{SFR}} < 10^{-2.9} \text{ M}_{\odot} \text{ yr}^{-1} \text{ kpc}^{-2}$  (95 % confidence level), which is less than the solar-neighborhood value of  $10^{-2.4} \text{ M}_{\odot} \text{ yr}^{-1} \text{ kpc}^{-2}$  (ref. 13).

As a result, we have detected an unusually strong magnetic field at  $z = 0.692$  with a coherence length that probably exceeds 200 pc in neutral gas that is quiescent, metal-poor, nearly dust-free, and presents little evidence for star formation. To model this configuration, we first consider the magnetostatic equilibrium of a plane-parallel sheet with in-plane magnetic field  $B_{\text{plane}}$  orthogonal to the vertical gravitational field exerted by gas with perpendicular mass surface density,  $\Sigma$ . In magnetostatic equilibrium the total midplane pressure,  $(B_{\text{plane}}^2/8\pi) + \rho\sigma_v^2$ , equals the ‘weight’ of the gas,  $\pi G\Sigma^2/2$ , where  $\rho$  is the mass volume density of the gas and  $G$  is the gravitational constant. However, because the pressure-to-weight ratio exceeds 715 in DLA-3C286, the magnetized gas cannot be confined by its self-gravity. Therefore, self-consistent magnetostatic configurations are ruled out unless the contribution of stars to  $\Sigma$  exceeds  $\approx 350 \text{ M}_{\odot} \text{ pc}^{-2}$ . Although this is larger than

the  $50 \text{ M}_{\odot} \text{pc}^{-2}$  surface density perpendicular to the solar neighborhood, such surface densities are common in the central regions of galaxies. In fact high surface densities of stars probably confine the highly magnetized gas in the nuclear rings of barred spirals. These exhibit *total* field strengths of  $\sim 100 \mu\text{G}$ , inferred by assuming equipartition of magnetic and cosmic-ray energy densities<sup>1</sup>. However, because the rings are associated with regions of active star formation, high molecular content, and high dust content, they are unlikely sites of the magnetic field detected in DLA-3C286.

On the other hand the absorption site might consist of highly magnetized gas confined by the gravity exerted by a disk of old stars. The H I disks found at the centers of early-type S0 and elliptical galaxies<sup>14</sup> are possible prototypes. Support for this idea stems from a high-resolution image obtained with the Hubble Space Telescope: a Wide Field and Planetary Camera 2 (WFPC2) *I*-band image, from which the quasar has been subtracted, reveals residual emission spread over angular scales of  $\sim 1''$  (ref. 15). The asymmetry of the light distribution with respect to the point-source quasar suggests that some of the light is emitted by a foreground galaxy with a brightness centroid displaced less than  $0.5''$  from the quasar. The location of diffuse emission in the direction of an amorphous object detected  $2.5''$  from the quasar in ground-based imaging<sup>16</sup> further suggests that the diffuse emission comes from central regions of the amorphous object. A recent reanalysis of the WFPC2 image shows the amorphous object to be a filament resembling a spiral arm or tidal tail (H.-W. Chen, personal communication), that is, the outer appendage of a galaxy centered within a few kpc of the quasar sightline.

However, the magnetic field detected in DLA-3C286 may not be confined by gravity in an equilibrium configuration. Rather, the detected field may be enhanced by a shock (F.H.Shu, personal communication). Assuming a typical value of  $B_{\text{plane}} \approx 5 \mu\text{G}$  for the equilibrium field of the preshock gas, we find that a shock-front velocity of  $\approx 250 \text{ km s}^{-1}$

will result in a post-shock field strength of  $\approx 100 \mu\text{G}$  in the limit of flux freezing in a radiative shock with post-shock density of  $\approx 10 \text{ cm}^{-3}$ . This scenario seems plausible because  $250 \text{ km s}^{-1}$  is reasonable for the impact velocity generated by the merger between the gaseous disks of two late-type galaxies, and the WFPC2 image is consistent with the presence of two foreground galaxies. But the second disk would create another set of absorption lines displaced  $\geq 250 \text{ km s}^{-1}$  from the redshift of DLA-3C286, which is the only redshift observed. By contrast, the merger between a gaseous disk and an elliptical galaxy could result in only one damped Ly $\alpha$  system redshift, as a significant fraction of ellipticals do not contain H I disks<sup>14</sup>. In this case a shock front moving in the plane of the disk galaxy would be generated by the gravitational impulse induced by the elliptical moving normal to the plane. Preliminary estimates indicate that an elliptical with a modest mass,  $M=2\times 10^{11} M_{\odot}$ , and impact velocity of  $\approx 300 \text{ km s}^{-1}$  would produce a cylindrical shock of sufficient strength to boost an initial field with  $B_{\text{plane}} \approx 10 \mu\text{G}$  to  $\approx 100 \mu\text{G}$ .

Let us examine these scenarios more closely. The quiescent velocity field of the gas fits in naturally with the ‘magnetostatic equilibrium’ scenario, because the low value of  $\Sigma_{\text{SFR}}$  suggests a low rate of energy injection into the gas by supernovae<sup>17</sup>, which could result in a velocity dispersion of  $\sigma_v \approx 4 \text{ km s}^{-1}$ . Moreover, the weak radio jets associated with early-type galaxies containing central H I disks are natural sources of  $B$  fields for these disks. However, 21 cm absorption measurements of such disks in nearby galaxies reveal the presence of absorption-line widths far broader than the narrow-line width of DLA-3C286 (ref. 18). Also, it is unclear whether or not the high surface density of old stars required to confine the  $B$  fields are present in these disks, and whether or not the build-up of  $B_{\text{plane}}$  to  $100 \mu\text{G}$  is possible in the 4 to 5 Gyr age of the disk. In the ‘merger scenario’ the dynamo need only build up to  $\approx 10 \mu\text{G}$  in the same time interval, but it is then necessary to explain why the post-shock velocity field averaged over length scales of 200 pc is so quiescent. Furthermore, the probability  $p$  for detecting  $\sim 100\text{-}\mu\text{G}$  magnetic fields in a random sample

of 21 cm absorbers is small. Our estimates, based on the merger fraction of galaxies with  $z \sim 1$  (ref. 19) and on the duration time for magnetic field enhancement, suggest that  $p \approx 0.005$  to  $0.03$ : either we were lucky, or some characteristic of DLA-3C286, such as narrow line width, is a signature of strong magnetic fields.

Therefore, it is premature to decide among these and other possible models to explain the presence of the  $84 \mu\text{G}$  magnetic field in DLA-3C286. However, our data support the inference from recent tentative evidence for Faraday rotation in high- $z$  quasars<sup>20</sup> that magnetic fields are generic features of galaxies at high redshifts, which potentially have a more important role in galaxy formation and evolution<sup>21</sup> than hitherto realized. Specifically, the highly magnetized gas that we have detected could suppress gravitational collapse and hence may be a reason for the low *in situ* star formation rates of high- $z$  DLAs<sup>22</sup>. We plan to test this hypothesis by using the GBT to search for Zeeman splitting in high-redshift DLAs exhibiting 21 cm absorption.

## REFERENCES

1. Beck, R. Magnetic fields in galaxies. *Lect. Notes. Phys.* **664**, 41-68 (2005).
2. Han, J. L., Manchester, R. N., Lyne, A. G., Qiao, G. J. & van Straten, W. Pulsar rotation measures and the large-scale structure of galactic magnetic fields. *Astrophys. J.* **642**, 868-881 (2006).
3. Kronberg, P. P., Bernet, M. L., Miniati, F., Lilly, S. J., Short, M. B. & Higdon, D. M. A global probe of cosmic magnetic fields to high redshifts. *Astrophys. J.* **676**, 70-79 (2008).
4. Heiles, C. & Troland, T. H. The millenium Arecibo 21 centimeter absorption-line survey. III. Techniques for spectral polarization and results for Stokes *V*. *Astrophys. J. Supp.* **151**, 271-297 (2004).
5. Parker, E. The origin of magnetic fields, *Astrophys. J.*, **160**, 383-404 (1970).
6. Brown, R. L. & Roberts, M. S. 21-centimeter absorption at  $z=0.692$  in the quasar 3C 286. *Astrophys. J.*, **184**, L7-L10 (1973).
7. Davis, M. M. & May, L. S. New observations of the radio absorption line in 3C 286, with potential application to the direct measurement of cosmological deceleration. *Astrophys. J.*, **219**, 1-4 (1978).
8. Wolfe, A. M., Gawiser, E., & Prochaska, J. X. Damped Ly $\alpha$  Systems. *Annu. Rev. Astron. Astrophys.*, **43**, 861-918 (2005).
9. Wolfe, A. M., Broderick, J. J., Condon, J. J., & Johnston, K. J. 3C 286: A cosmological QSO? *Astrophys. J.*, **208**, L47-L50 (1976).



10. Meiring, J. D., Kulkarni, V. P., Khare, P., Bechtold, J., York, D. G., Cui, J., Lauroesch, J. T., Crotts, A. P. S., & Nakamura, O. Elemental abundance measurements in low-redshift damped Ly $\alpha$  absorbers. *Mon. Not. R. Astron. Soc.*, **370**, 43-62 (2006).
11. Wolfe, A. M., & Prochaska, J. X., & Gawiser, E. CII\* absorption in damped Ly $\alpha$  systems. I. Star formation rates in a two-phase medium. *Astrophys. J.*, **593**, 215-234 (2003).
12. Boisse, P., Le Brun, V., Bergeron, J., Deharveng, J.-M. A HST spectroscopic study of QSOs with intermediate redshift damped Ly $\alpha$  systems. *Astron. Astrophys.*, **333**, 841-863 (1998).
13. Kennicutt, R. C., Jr. Star formation in galaxies along the Hubble sequence. *Annu. Rev. Astron. Astrophys.*, **36**, 189-231 (1998).
14. Morganti, R. et al. Neutral hydrogen in nearby elliptical and lenticular galaxies: the continuing formation of early-type galaxies. *Mon. Not. R. Astron. Soc.*, **371**, 157-169 (2006).
15. Le Brun, V., Bergeron, J., & Deharveng, J. M. The nature of intermediate-redshift damped Ly $\alpha$  absorbers. *Astron. Astrophys.*, **321**, 733-748 (1997).
16. Steidel, C. C., Pettini, M., Dickinson, M., & Persson, S. E. Imaging of two damped Lyman-alpha absorbers at intermediate redshifts. *Astron. J.*, **108**, 2046-2053 (1994).
17. McKee, C. F. & Ostriker, J. P. A theory of the interstellar medium: three components regulated by supernova explosions in an inhomogeneous substrate. *Astrophys. J.*, **218**, 148-169 (1977)
18. Morganti, R., Greenhill, L. J., Peck, A. B., Jones, D. L. & Henkel, C. Disks, tori, and

- cocoons: emission and absorption diagnostics of AGN environments. *New Astron. Rev.*, **48**, 1195-1209 (2004).
19. Lotz, J. M., et al. The evolution of galaxy mergers and morphology at  $z < 1.2$  in the extended Groth strip. *Astrophys. J.*, **672**, 177-197 (2008).
  20. Bernet, M. L., Miniati, F., Lilly, S. J., Kronberg, P. P. & Dessauges-Zavadsky, M. Strong magnetic fields in normal galaxies at high redshift. *Nature* **454**, 302-304 (2008)
  21. Rees, M. J. origin of cosmic magnetic fields. *Astron. Nachr.* **327**, 495-398 (2006)
  22. Wolfe, A. M. & Chen, H.-W. Searching for low surface brightness galaxies in the Hubble ultra deep field: implications for the star formation efficiency in neutral gas at  $z \sim 3$ . *Astrophys. J.*, **652**, 981-993 (2006).
  23. Heiles, C. Cross-correlation spectropolarimetry in single-dish radio astronomy. *Pub. Astron. Soc. Pac.* **113**, 1243-1246 (2001).
  24. Baym, G. *Lectures on quantum mechanics* Ch. 1 (W. A. Benjamin Inc. Reading, Mass. 1981).
  25. Savage, B. D., & Sembach, K. R., Interstellar abundances from absorption- line observations with the Hubble-Space Telescope *Annu. Rev. Astron. Astrophys.*, **34**, 279-329 (1996).

**Acknowledgements** We wish to thank F. H. Shu for suggesting the merger model and H.-W. Chen for providing us with her reanalysed images of 3C 286.. We also thank F. H. Shu, E. Gawiser, and A. Lazarian for comments and the US National Science

Foundation for financial support. The GBT is one of the facilities of the National Radio Astronomy Observatory, which is a center of the National Science Foundation operated under cooperative agreement by Associated Observatories, Inc. A. M. W., R. A. J., and J. X. P. are Visiting Astronomers at the W. M. Keck Telescope. The Keck Observatory is a joint facility of the University of California, the California Institute of Technology and the National Aeronautics and Space Administration.

Redshift $z=0.69217485\pm0.00000058$		
Velocity Dispersion $\sigma_v=3.08\pm0.13$ km s <sup>-1</sup>		
Ion $X$	$\log_{10}N(X)$ cm <sup>-2</sup>	[X/H]
H I	$21.25\pm0.02$	—
Fe II	$15.09\pm0.01$	$-1.66\pm0.02$
Cr II	$13.44\pm0.01$	$-1.48\pm0.02$
Zn II	$12.53\pm0.03$	$-1.39\pm0.03$
Si II	$> 15.48$	$> -1.31$

Table 1: **Physical Parameters of DLA-3C286 Inferred from Optical Absorption**

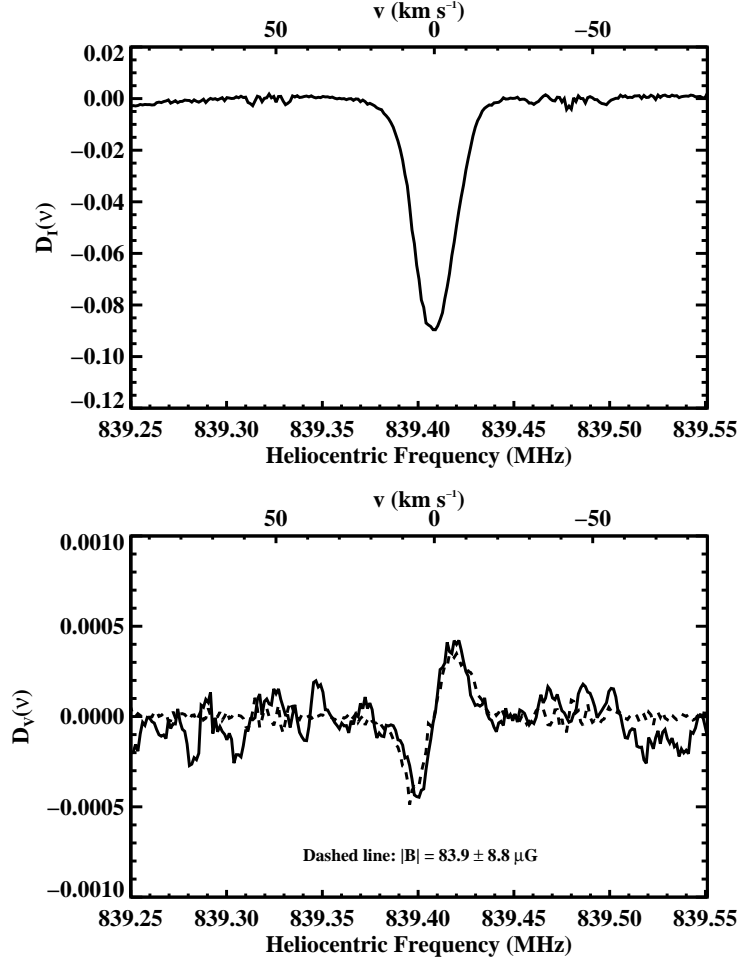


Fig. 1.— **Line-depth spectra of Stokes-parameters.** Data acquired in 12.6 hrs. of on-source integration with the GBT radio antenna. Because the GBT feeds detect only orthogonal linearly polarized signals, while Zeeman splitting requires measuring circular polarization to construct Stokes  $V(\nu)$ , we generated  $V(\nu)$  by cross-correlation techniques<sup>23</sup>. The velocity  $v=0 \text{ km s}^{-1}$  corresponds to  $z=0.6921526$ . **a**, Line-depth function  $D_I(\nu) \equiv [I(\nu) - I_c(\nu)]/I_c(\nu)$ , where  $I(\nu) \equiv s_0 + s_{90}$ , with  $s_\theta$  the power measured in linear polarization position angle  $\theta$ , corresponds to the total intensity spectrum, and  $I_c(\nu)$  is a model fit to the  $I(\nu)$  continuum.  $D_I(\nu) = \exp[-\tau(\nu)] - 1$  where  $\tau(\nu) \equiv [\tau(\nu)_0 + \tau(\nu)_{90}]/2$  is the average optical depth in the two orthogonal states of linear polarization<sup>4</sup>. **b**, Line-depth function  $D_V(\nu) \equiv V(\nu)/I_c(\nu)$ , where  $V(\nu) \equiv s_{\text{RCP}} - s_{\text{LCP}}$  is difference in power between the right-hand and left-hand circularly polarized (respectively RCP and LCP) signals. Here  $D_V(\nu) = -[\tau_V(\nu)/2]\exp[-\tau(\nu)]$ , where  $\tau_V(\nu) \equiv \tau_{\text{RCP}}(\nu) - \tau_{\text{LCP}}(\nu) \ll 1$  (ref. 4) is the difference between the optical depths of RCP and LCP photons. For Zeeman splitting of the 21 cm line, the degeneracy of the  $F = 0$  to  $F = 1$  hyperfine transition is removed since the  $m_F = -1, 0, +1$  states differ in energy. This results in a small frequency difference between absorbed LCP photons ( $m_F = -1$ ) and RCP photons ( $m_F = +1$ ).  $V(\nu)$  is crucial for detecting Zeeman splitting because the orthogonal, circularly polarized states of the photon are eigenstates of the spin angular momentum operator with eigenvalues  $\pm \hbar$ , that is, angular momenta directed along or opposite to the direction of photon propagation.<sup>24</sup> When  $B_{\text{los}} = B$ , transitions between the hyperfine  $F = 0$  and  $F = 1$  states occur exclusively through absorption of LCP or RCP photons through excitation of the  $m_F = -1$  and  $m_F = +1$  hyperfine states respectively. Because  $V(\nu)$  is the difference in the RCP and LCP intensities, the resulting  $V(\nu)$  line profile is the difference between two Gaussian absorption profiles with frequency centroids shifted by  $\Delta\nu_B = 2.8(B_{\text{los}}/\mu\text{G})(1+z)^{-1} \text{ Hz}$  (where  $B_{\text{los}}$  is measured in microgauss). The ‘S curve’ is due to the sign flip in RCP-minus-LCP intensity difference as  $\nu$  passes through line centre.

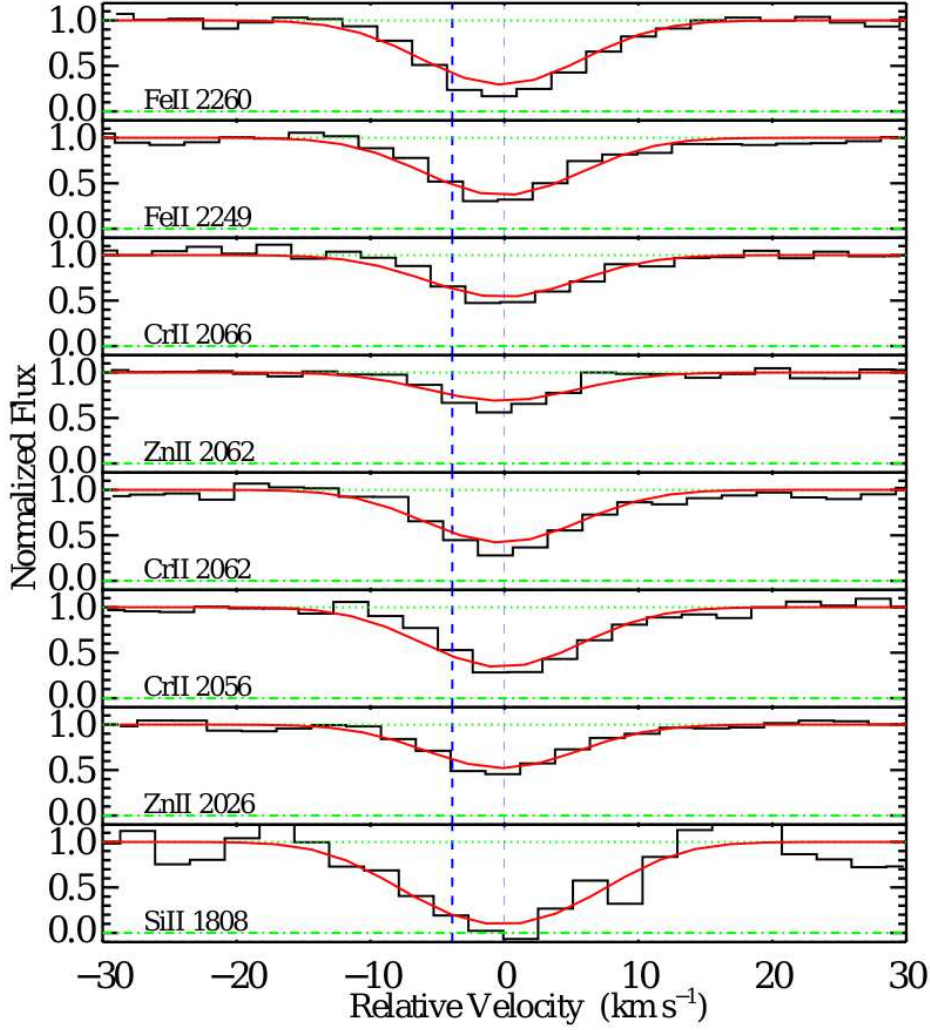


Fig. 2.— Hires velocity profiles for dominant low-ionization states of abundant elements in the 21 cm absorber towards 3C 286. Spectral resolution  $\Delta v=7.0 \text{ km s}^{-1}$  and the average signal-to-noise ratio per  $2.1 \text{ km s}^{-1}$  pixel is about 30:1. The bold dashed vertical line denotes the velocity centroid of single-dish 21 cm absorption feature and the faint dashed vertical line denotes the velocity centroid of the resonance lines shown in the figure. Our least squares fit of Voigt profiles (red) to the data (black) yields ionic column densities as well as the redshift centroid and velocity dispersion shown in Table 1 (lower and upper green horizontal lines refer to zero and unit normalized fluxes). Because refractory elements such as Fe and Cr can be depleted onto dust grains<sup>25</sup>, we used the volatile elements Si and Zn to derive a logarithmic metal abundance with respect to solar abundances of  $[M/H]=-1.30$ . The depletion ratios  $[Fe/Si]$  and  $[Cr/Zn]$  were then used to derive a conservative upper limit on the logarithmic dust-to-gas ratio relative to Galactic values of  $[D/G] < -1.8$ .